Low-velocity impact responses and CAI properties of synthetic foam sandwiches

Jun Wang[1], Jing Li[1], Hota GangaRao[2], Ruifeng Liang[2], Jiye Chen[3]

[1]College of Civil Engineering, Nanjing Tech University, Nanjing, People's Republic of China
[2]Department of Civil and Environmental Engineering, West Virginia University, WV, USA
[3] School of Civil Engineering and Surveying, University of Portsmouth, UK

Abstract: This paper presents experimental and analytical studies on impact and compression after impact (CAI) responses of synthetic foam sandwiches with glass fiber reinforced polymer (GFRP) skins and synthetic foam cores under low-velocity impacting. The impact test results showed that the penetration depth of GFRP panels with synthetic foam is much smaller than that of bare synthetic foam panels. The edgewise compression test results indicated the facesheet debonding dominates the failure mode of the sandwich panels without lattice webs, while the failure mode of the sandwich panels with lattice webs is predominated by the wrinkling and delamination of the facesheets and the crushing of foam core. The influences of applied impact energy, GFRP lay-up, synthetic foam density and the existence of webs on the impact and post impact behavior of sandwich panels are discussed herein. Analytical models are proposed to predict the residual ultimate edgewise compressive load capacity of sandwich panels with lattice webs after impacts, using energy principles and variational methods in applied mechanics. The influences from impact damage, the local buckling of the facesheets and the confined strength of the foam core are measured and compared well with proposed analytical models.

Key words: Sandwich; Composites; Synthetic foam; Low-velocity impact; Compression after impact (CAI)

1. Introduction

Sandwich composites with high stiffness are able to carry more loads and absorb more energy. This is attributed to their lightweight, high flexural and transverse shear stiffness, and good environmental resistance over solid sections [1-3]. However, they are susceptible to low-velocity impacts, which would result a sudden structural destruction [4]. Synthetic foam consisting of fillers with hollow cores is one of the promising core materials for sandwiches, providing superior compressive strength, high damage tolerance and excellent energy absorption [5]. This synthetic foam sandwiches withsynthetic hollow core have potential to be widely used in marine structures, transportations and civil infrastructures, however,their applications require fully understanding their failure mechanism under low-velocity impacting and reliably assessing their damage tolerance.

Composite sandwich panels: The impact behavior of sandwich composites has attracted attention from many researchers. Xia and Wu [6] studied low-velocity impact responses of sandwich composites with different types of fiber reinforced polymer (FRP) skins. Their test results showed that sandwiches with Kevlar facesheet

have the largest average damage angle and the smallest cracking width and dent depth, compared to those sandwiches with glass, carbon, and carbon/Kevlar hybrid facesheets. Ugale et al. [7] compared the impact responses of GFRP thin sandwich panels (thickness of 2.5 mm) and carbon fiber reinforced polymer (CFRP) thin sandwich panels with polyester foam Coremat XM. The CFRP thin sandwich panel was penetrated under the applied impact energy of 18 J while the GFRP thin sandwich panel was not penetrated because of its higher elastic deflection and lower stress [7]. Low-velocity impact causes various forms of damages in sandwich structures and results in a severe reduction in compressive, shear and bending strengths, in which the residual compressive strength is most susceptible to the impact [8-10]. Zhu and Chai [11] investigated the damage modes and failure modes of CFRP-Nomex honeycomb core sandwich panels under low velocity impact. They found that the facesheet thickness and the core density affected the failure modes significantly while the latter had insignificant effects on ultimate load capacity. The test results of Schubel et al. [8] showed that the sandwich panels containing delamination in the impacted facesheets had edgewise compressive strength which is less than the half of the original strength. The reduction of residual compressive strength of sandwich panels with CFRP skins (60.8%) is far greater than that of panels with GFRP skins (14.3%) [12]. Castanie [13] proposed a core crush criterion to analyze the nonlinear impact response and predicted the residual strength of sandwich composite structures with impact damage. The experimental study of Nettles [14] showed that dividing the impact energy by the facesheet thickness to powers of 2.0 and 2.5 gave more comparable strength under compression after impact (CAI) than the power of 1.0 for composite sandwich panels with 8-, 16- and 24-ply facesheet laminates (nominal laminate thickness of 1.09, 2.18 and 3.28 mm). Feng and Aymerich [15] modeled the typical damage modes of CFRP-PVC foam sandwich panels under low-velocity impact through finite element methods, in which the nonlinear behavior of the foam core was modeled by a crushable foam plasticity model.

Metal sandwich panels: In order to improve the impact performance of sandwiches with aluminum honeycomb core, Sabah et al. [16] developed a novel sandwich beam in which a layer of rubber was inserted between the honeycomb core and facesheets, resulting in an impact resistance 2.7-5.7 times higher than that of conventional sandwich beams. Crupi et al. [17] compared the impact responses of aluminum foam sandwiches reinforced with and without GFRP skins. They found that the debonding of the aluminum face from the core dominated the failure mode of specimens reinforced with GFRP skins, whereas the foam core crushing dominated the failure mode of specimens without GFRP skins. Chen et al. [18] developed numerical models to predict the intra-laminar damage, inter-laminar and adhesive delamination and core crushing of composite sandwich structures under low-velocity. Hassan et al. [19] compared the impact responses of GFRP/aluminium honeycomb sandwich panels and self-reinforced polypropylene (SRP)/ polypropylene (PP) honeycomb sandwich panels. Their test results showed that with the increase of skin thickness, the specific perforation energy (SPE) of GFRP/aluminium sandwiches remained approximately

constant while the SPE of SRP/PP sandwiches increased rapidly, and the SPE of GFRP/aluminium sandwiches was much lower than that of SRP/PP sandwiches [19].

Synthetic foam sandwich panels: Although sandwiches with polymer foam exhibit higher SPE than metal foam sandwiches, the polymer foam sandwiches have no overwhelming superiority on the impact resistance compared with metal sandwiches under the same weight. Using synthetic foam as sandwich core can increase the stiffness and strength of sandwiches significantly without a large weight increase [20]. Lamanna et al. [21] investigated the dynamic characterization of aluminum synthetic foam sandwich composites with CFRP skins based on free vibration method. Kumar and Ahmed [22] developed a stiffening phenolic synthetic foam core by the incorporation of resin impregnated paper honeycomb (RIPH), resulting in a 60% enhancement of energy absorption. Omar et al. [23] studied the compressive property of aluminum synthetic foam sandwich composites at quasi-static and high strain rates. Their test results revealed that the CFRP skin had a reinforced effect under quasi-static conditions, while the compressive strength of the sandwich was similar to that of bare synthetic foam core in the strain range 525-845/sec. Bardella et al. [24] proposed a micromechanical model to capture the quasi-brittle failure of synthetic foams under compression. Using synthetic foam as core can fully utilize the mechanical properties of both synthetic foams and FRPs, and avoid debonding between the core and facesheets.

Although some focus were given on the static and impact responses of synthetic foam sandwiches in several studies, the residual strength of synthetic foam sandwiches after impact has received scant attention. For synthetic foam sandwiches applied as load bearing elements or energy absorbers, it is necessary to estimate their damaged conditions and load carrying capacities after impact. Therefore, the present study focuses on characterizing the impact damage and the residual compression strength of sandwich panels with GFRP facesheets, and the influence of macrospheres embedded in epoxy matrix synthetic foam core after low-velocity impact. Influences of the number of GFRP skin layers, synthetic foam density including lattice webs, as well as the applied impact energy are discussed in this paper. Analytical models are developed to predict residual ultimate load capacity of synthetic foam sandwich panels with longitudinal and transversal webs after impact, using classical energy principles in mechanics of materials.

2. Experimental program

2.1 Materials and test specimens

E-glass bidirectional woven fabrics with fiber orientation angle 0/90° and vinyl ester resin were used in facesheets with 0.6 mm thickness and lattice webs. The synthetic foams were cut into blocks with specific dimensions to fit test specimen sizes, and wrapped with GFRP fabrics. Vacuum assisted resin infusion process was used to manufacture GFRP- synthetic foam sandwich panels with and without lattice webs. The fiber longitudinal -transversal volume fraction is 1:1 in both the facesheets and

webs. To determine the material properties of GFRP composites, tensile and compressive tests were conducted in accordance with ASTM D 638-10 [25] and ASTM D 695-15 [26]. The measured properties of the composite materials are given in Table 1.

The macrosphere synthetic foams, supplied by Engineered Synthetic Systems, USA, with density of 450 kg/m^3 and 480 kg/m^3 were used in this study. The compressive properties of the synthetic foams were measured in accordance with ASTM D 1621-10 [27]. The test results showed that the synthetic foam with density of 450 kg/m^3 has compressive strength of 22 MPa and Young's modulus of 1 GPa, and the synthetic foam with density of 480 kg/m^3 has compressive strength of 25 MPa and Young's modulus of 2.5 GPa.

A total of 40 specimens were prepared to study the influence of impact damage on the residual strength, including 8 bare synthetic foam panels, 16 GFRP- synthetic foam sandwich panels without webs, and 16 GFRP- synthetic foam sandwich panels with transverse and longitudinal webs. The distance between the webs is 50 mm. Fig.1 shows the sketch of the sandwich panels with lattice webs. All the test specimens are of the same width of 100 mm, length of 150 mm and core height of 50 mm. The differences between the test specimens are the number of layers of the FRP facesheets, the density of synthetic foams and applied impact energy, as well as the existing of the GFRP facesheets and webs. Table 2 lists the details of the test specimens.

2.2 Impact testing

DTM1203 drop-weight impact testing machine was used to impact the specimens at room temperature. The maximum drop height is 2 m. The impactor has a semicircular nose with a diameter of 16 mm. During testing, the drop hammer with a mass of 5.5 kg is raised automatically by an automatic control system. Four different drop heights were used (0, 0.8 m, 1.2 m and 2 m), in which the applied energy can be varied from 0 to 108 J. Each specimen was impacted only once. Four corners of the test specimens were clamped to avoid slippage and rotation. Fig. 2 shows the test set up of low-velocity impact.

The time histories of impact loads were captured with a piezoelectric sensor mounted onto the drop hammer. The maximum penetration depth (MPD) after impact was measured by a micrometer with a resolution of 0.01 mm.

2.3 CAI testing

A universal testing machine with 600 kN capacity was used for testing edgewise compressive strength of damaged and undamaged specimens. During testing, the compressive load was applied through a very stiff steel top panel with the load rate of 1.25 mm/min, and was collected via a load cell mounted directly on the top panel. The displacement of crosshead was recorded by the actuator automatically. Steel fixture systems were applied to both ends of the sandwich columns to minimize the stress

concentrations of the facesheets at the contact with loading panels and to ensure uniform load transfer. In accordance with ASTM D7137/7127M-12 [28], all the specimens were loaded until the maximum load was reached and load application was continued till the residual load reduced 70% of its maximum load value. The test set-up of edgewise compression was shown in Fig.3.

3. Results and discussion

3.1 Impact responses

The bare synthetic foam panels exhibited a circular dent on the impact face, as shown in Fig.4 (a). The increase in applied impact energy from 41 J to 108 J leads to 61% ~ 76% increments in the maximum penetration depth (MPD) for bare synthetic foam panels. Under the same applied impact energy, the MPD of synthetic foam panels with foam density of 450 kg/m^3 is 20%~40% higher than the panels with foam density of 480 kg/m^3.

For GFRP- synthetic foam sandwich panels without webs under the applied impact energy 41 J, the damage is concentrated in the facesheets and has a diamond shape due to the breakage of fibers in the longitudinal and transverse directions, as shown in Fig.4(b). The deformation of the core in the impact zone is insignificant. However, when increasing applied impact energy, the shape of damaged area changes to be a circle because the resin is crushed by the semicircular nose of the impactor and delamination occurs in the FRP layers. The facesheets in the loading location is penetrated into the core resulting in a deeper MPD in the foam core. When the applied impact energy increased from 41 J to 108 J, the MPD increased by 121% to 646% for synthetic sandwich panels with varied number of layers of GFRP facesheets from 2 to 6. Although the increment of applied impact energy leads to remarkable increases in MPD of sandwich panels, the MPD of sandwich panels is much smaller than that of bare synthetic foam panels.

The damage mode of GFRP- synthetic foam sandwich panels with webs is similar to those sandwiches without webs, as shown in Fig.4(c). However, the sandwich panels with webs have smaller damage width and penetration depth than the counterparts without webs. When the applied impact energy increased from 41 J to 108 J, the MPD increased by 260% to 323% for synthetic sandwich panels with varied number of layers of GFRP facesheets from 2 to 6 and lattice webs. The MPD of sandwiches with webs at 41 J is almost the same as that of counterparts without webs, while the MPDs of sandwiches with webs at 81 J and 108 J are much less than those of counterparts without webs.

The impact load-time history curves of test specimens exhibit similar half-sinusoidal profile (Fig.5). Increment of the number of layers of facesheets from 0 to 6 leads to a 118% increment of the peak load and a 35% reduction of the duration for specimens at 108 J. When the applied impact energy increased from 41 to 108 J, the peak load and duration increased by 33% and 12%, respectively, for bare synthetic foam panels,

increased by 20%~41% and 3%~23%, respectively, for sandwich panels without webs, and increased by 27%~45% and 5%~15%, respectively, for sandwich panels with webs. The peak load increased up to 16% for sandwich panel with webs compared with the counterparts without webs. Moreover, the specimens with 4 layers of facesheets and webs had a shorter duration than the counterparts without webs, while the specimens with 6 layers of facesheets and webs had a longer duration than the counterparts without webs. In addition, the peak impact load and duration have no significant difference in responses of synthetic foam panels with and without GFRP facesheets at different foam densities. The impact responses of all the test specimens are shown in Table 2.

Given the same thickness of core and skins, the peak load of impact of GFRP-synthetic foam sandwiches is about two times of that of GFRP-polymethacrylimide (PMI) foam sandwiches under 40 J in Ref [9], and the corresponding MPD of GFRP-synthetic foam sandwiches is much smaller than that of GFRP- PMI foam sandwiches.

3.2 Undamaged sandwich panel under compression

Fig.6 shows the conditions of undamaged specimens after edgewise compression. For bare synthetic foam specimens, the transversal cracks initiated at the mid-height of the specimens, and then propagated to the margin. The synthetic foam sandwich specimens without webs failed with the debonding between the facesheets and core and vertical cracks in the foam core. For synthetic foam sandwich specimens with webs, the debonding between the facesheets and core is partially controlled by the webs and the facesheets wrinkled due to the local buckling. Moreover, vertical cracks of the foam core are restrained at the central region of the specimens by the webs. The edgewise compressive strength of undamaged specimens is then compared with the CAI strength of the damaged specimens.

3.3 Damaged sandwich panel under compression

Fig.7 shows the conditions of damaged specimens after edgewise compression. The cracks of damaged synthetic foam specimens are initiated from the impact dent due to the stress concentration in this region, and propagated in transversal and vertical directions, as shown in Fig.7(a). For damaged sandwich specimens without webs, widespread debonding between the facesheets and core occurred on both sides accompanied by vertical crack propagation in the foam core. The sandwich columns without webs are failed due to the facesheets being buckled into a half-wave and shear buckling of the foam core, as shown in Fig.7(b). The failure mode of damaged sandwich columns with webs is comprised by the debonding of facesheets, core being crushed between two webs, as well as delamination in GFRP layers, especially in the facesheets with impact damages. The debonded area of panels with webs is much smaller than thedebonded area of panels without webs because the debonding between the facesheets and the foam is controlled by the webs. Meanwhile, wrinkling occurred at the intersection of facesheets and webs. The indentation on the facesheets

under edgewise compression propagated to the intersection of facesheets and the upper web until the stress in this intersection reached to its critical value, resulting in local buckling in the upper intersection. Then the indentation continued to propagate to the intersection of facesheets and the lower web, and caused local buckling at this intersection. This wrinkling process not only causes the delamination of facesheets, but also results in shear buckling of the foam core between two webs, as shown in Fig.7(c).

The typical compressive load vs. displacement curves of bare synthetic foam panels and FRP- synthetic foam sandwich panels are shown in Fig.8. Both the intact and impacted bare synthetic foam panels exhibited brittle failure under edgewise compression. The load on synthetic foam panels increases linearly to its peak then the panels lost their load carrying capacities suddenly. In contrast to bare synthetic foam specimens, the sandwich specimen without webs underwent a short plastic phase after the linear-elastic phase which is associated with the crushing of the foam, then the load increased due to compaction of the foam core and facesheets until total separation of facesheets from the core. Finally, the sandwich specimens lost their load carrying capacities due to buckling of facesheets and the core. For sandwich specimens with webs, they have a much larger plastic deformation than the specimens without webs and their load carrying capacities decreased gradually, which indicates they are suitable to be applied as energy absorption members.

The ultimate load of impacted bare synthetic foam panels after 108 J is reduced less than 8% in comparison with the intact panels. Although the damage depth of sandwich panels is much lower than that of bare synthetic foam panels, the ultimate load of impacted sandwich panels with and without webs after 108 J is reduced by 8% to 14% in comparison with the intact panels. This is attributed to the fact that the impact dent aggravates the debonding between facesheets and core, and delamination between GFRP layers.

4. Prediction of residual load capacity

4.1 Local buckling of the facesheets

The local buckling of a facesheet strengthened by lattice webs can be analyzed based on the theory of elastic stability, as shown in Fig.9.

It is assumed that the top and bottom edges (z=0 and z=a) of the facesheets have no deformation in the y direction. Thus, the deflected surface of a buckled facesheet strengthened by lattice webs can be taken in the form of a double trigonometric series, as given by Timoshenko and Gere [29]

$$w = \sum_{m=1}^{\infty} a_m \sin\frac{m\pi z}{a} \sin\frac{\pi x}{b} \tag{1}$$

where a and b are the length and width of the facesheets, respectively.

The potential energy of bending of a facesheet is given by Timoshenko and Gere [29]

$$U=\frac{1}{2}D\iint\left\{\left(\frac{\partial^2 w}{\partial x^2}+\frac{\partial^2 w}{\partial y^2}\right)^2-2(1-\nu)\left[\frac{\partial^2 w}{\partial x^2}\frac{\partial^2 w}{\partial y^2}-\left(\frac{\partial^2 w}{\partial x\partial y}\right)^2\right]\right\}dxdy \tag{2}$$

where D is the flexural rigidity of the facesheets and ν is Poisson's ratio
Substituting Eq. (2) to Eq. (1), the strain energy of bending of a facesheet can be achieved as (Timoshenko and Gere 1961)

$$\Delta U=\frac{\pi^4 D}{2}\frac{ab}{4}\sum_{m=1}^{\infty}a_m^2\left(\frac{m^2}{a^2}+\frac{1}{b^2}\right)^2 \tag{3}$$

Considering the restraint effects of foam core on the facesheets, the foam is represented by the springs with a stiffness of k (per unit width and length) and we assumed that the facesheets are supported on the elastic foundation. Thus, the energy associated with elastic foundation is

$$\Delta U_f=\frac{1}{2}\int_0^b\int_0^a kw^2dxdz=\frac{abk}{8}\sum_{m=1}^{\infty}a_m^2 \tag{4}$$

For a longitudinal web at distance c_i from the edge x=0, the web bending strain energy when buckled together with the facesheet, is

$$\Delta U_i^L=\frac{EI_i}{2}\int_0^a\left(\frac{\partial^2 w}{\partial z^2}\right)^2\Bigg|_{x=c_i}dx=\frac{\pi^4 EI_i}{4a^3}\sum_{m=1}^{\infty}m^4a_m^2\sin^2\frac{\pi c_i}{b} \tag{5}$$

where E is the modulus of elasticity and I_i is the moment of inertia of the longitudinal of webs.
For a transversal web at the distance d_i from the edge z=0, the strain energy of bending of the web, when buckling together with the facesheets, is

$$\Delta U_i^T=\frac{\pi^4 EI_i^{'}}{4b^3}\left(\sum_{m=1}^{\infty}a_m\sin\frac{m\pi d_i}{a}\right)^2 \tag{6}$$

where $I_i^{'}$ is the moment of inertia of transversal webs.
The work done during buckling by the compressive load N_z acting on a facesheet is

$$\Delta T=\frac{N_z ab}{8}\sum_{m=1}^{\infty}\frac{m^2\pi^2}{a^2}a_m^2 \tag{7}$$

The work done during buckling by the compressive load P_i acting on a longitudinal web is

$$\Delta T_i^L=\frac{P_i}{2}\int_0^a\left(\frac{\partial^2 w}{\partial z^2}\right)_{x=c_i}^2dx=\frac{\pi^2 P_i a}{4a^2}\sum_{m=1}^{\infty}m^2a_m^2\sin^2\frac{\pi c_i}{b} \tag{8}$$

Based on the principle of energy conservation, the general equation for calculating the critical stress is

$$2\Delta U+\sum\Delta U_i^L+\sum\Delta U_i^T+\Delta U_f=2\Delta T+\sum\Delta T_i^L \tag{9}$$

where n is the number of facesheets. In this paper, n=2 and each facesheet has the same thickness.

Using the notations

$$\frac{P_i}{bN_x}=\delta_i;\quad \frac{a}{b}=\beta;\quad \frac{EI_i}{bD}=\gamma_i;\quad \frac{EI_i^{'}}{bD}=\gamma_i^{'}$$

and using the notation

$$\sigma_{cr}=\frac{(N_z)_{cr}}{h}$$

where h is the thickness of a facesheet, Eq. (10) can be resulted from Eq.(9)

$$\sigma_{cr}=\frac{\pi^2 D}{b^2\beta^2 h}\mathrm{g}$$

$$\frac{\left[n\sum_{m=1}^{\infty}a_m^2\left(m^2+\beta^2\right)^2+\sum_i 2\gamma_i\sum_{m=1}^{\infty}m^4a_m^2\sin^2\frac{\pi c_i}{b}+\sum_i 2\beta^3\gamma_i^{'}\left(\sum_{m=1}^{\infty}a_m\sin\frac{m\pi d_i}{a}\right)^2+\frac{k\sum_{m=1}^{\infty}a_m^2}{\pi^4\beta^4b^4D}\right]}{n\sum_{m=1}^{\infty}m^2a_m^2+2\sum_i\delta_i\sum_{m=1}^{\infty}a_m^2m^2\sin^2\frac{\pi c_i}{b}} \tag{10}$$

The minimum value of σ_{cr} can be obtained by equating to zero the derivatives of Eq. (10) with respect to the coefficients a_{m}, as given by

$$\frac{\partial\sigma_{cr}}{\partial a_m}=0 \tag{11}$$

From Eq. (11), it can be obtained as below.

$$\frac{\pi^2 D}{b^2 h}\left[na_m\left(m^2+\beta^2\right)^2+\sum_i 2a_m\gamma_i m^4\sin^2\frac{\pi c_i}{b}+\sum_i 2\beta^3\gamma_i^{'}\sin\frac{m\pi d_i}{a}\sum_{p=1}^{\infty}a_p\sin\frac{p\pi d_i}{a}+\frac{ka_m}{\pi^4 D\beta^4b^4}\right]$$
$$=\beta^2\sigma_{cr}\left[nm^2a_m+\sum_i 2\delta_i a_m m^2\sin^2\frac{\pi c_i}{b}\right] \tag{12}$$

σ_{cr} can be determined by equating to zero the determinant of this system of equations. In the case of sandwiches with two facesheets, two longitudinal webs and two transverse webs, we have n=2, d_1/a =1/3, d_2/a=2/3, c_1/b=1/4 and c_2/b=3/4. Moreover, it is assumed that the facesheets buckle into one half-wave and m is taken as 1[27]. Then

$$\sigma_{cr}=\frac{\pi^2 D}{2b^2 h}\mathrm{g}\frac{2\left(1+\beta^2\right)^2+2\gamma_1+3\beta^3\gamma_1^{'}+\frac{k}{\pi^4 D\beta^4b^4}}{\beta^2\left(1+\delta_1\right)} \tag{13}$$

4.2 Ultimate compressive load capacity of undamaged panels

The sandwich panels under edgewise compression can be considered as consisting of foam core confined by lattice webs and unconfined core, as shown in Fig. 9(b). The

compressive strength of the confined synthetic foam core can be expressed as [30]

$$\frac{f_c^{'}}{f_c} = 1 + k_1 k_s \frac{f_l}{f_c} \tag{14}$$

where $f_c^{'}$ and f_c are the compressive strength of synthetic foam confined with and without FRP, respectively, k_1 is the confinement effectiveness coefficient, which is taken as 0.93 for foam core[31], f_l is the lateral confining pressure of FRP and k_s is the shape factor.

The applied compressive load on the composite columns (P) is the sum of the loads on the FRP facesheets (P_f), longitudinal webs (P_w), confined foams (P_{cc}) and unconfined foams (P_c). Thus, the ultimate compressive load capacity of the panels without local buckling is expressed as

$$P_1 = 0.8 f_F A_f + 0.8 f_F A_w + f_c^{'} A_c^{'} + f_c A_c \tag{15}$$

where 0.8 is design facor for FRP [30], f_F is the compressive strength of FRP, A_f and A_w are the areas of FRP facesheets and longitudinal webs, respctively, and $A_c^{'}$ and A_c are the areas of the confined foam and unconfined foam, respectively.

The ultimate compressive load capacity of the panels with the local buckling of FRP facesheets is expressed as

$$P_2 = \sigma_{cr} A_f + 0.8 f_F A_w + f_c^{'} A_c^{'} + f_c A_c \tag{16}$$

where σ_{cr} is obtained from Eq.(13).

In practical design, the ultimate compressive load capacity of the panels P_u is the lesser of P_1 and P_2

$$P_u = \min (P_1, P_2) \tag{17}$$

4.3 Residual ultimate compressive load capacity of damaged panels

The strength and moduli retention ratios ξ_1 and ξ_2 are used to account for the effects of impact on the FRP. According to Ref. [32], the residual compression strength of GFRP laminates under the applied impact energies of 45 J and 68 J are about 75% and 60% of compressive strength of the undamaged GFRP laminates, respectively. There is a lack of the residual compression strength of GFRP laminates under the applied impact energy of 108J, so the reduction of CFRP properties after impact is used herein. Schubel et al. [8] reported that the reduction of compressive strength of CFRP facesheets under the applied impact energies of 108J aree about 70% of compressive strength of the undamaged CFRP laminates. Thus, the value of ξ_1 is taken as 0.75, 0.6 and 0.3 for FRP subjected to impact of 45 J, 68 J and 108 J. Moreover, as mentioned in Ref. [33], the moduli retention ratio is in the range of 0.11 and 0.19, which is related to the impact damage areas. Thus, ξ_2 is taken as 0.11, 0.15 and 0.19 for FRP subjected to impact of 45 J, 68 J and 108 J. Because the damage on the foam core is small, so the reduction on the mechanical properties of the foam core is negligible.

For a sandwich panel with impact damage on a facesheet, the buckling stress can be obtained based on Eq. (13), as given by

$$\sigma_{cr}^{'} = \frac{\pi^2 D}{2b^2 h} \mathrm{g} \frac{2\left(1+\beta^2\right)^2 + 2\frac{\gamma_1}{\xi_2} + 3\beta^3 \frac{\gamma_1^{'}}{\xi_2} + \frac{k}{\pi^4 \xi_2 D \beta^4 b^4}}{\beta^2\left(1+\delta_1\right)} \tag{18}$$

The compressive strength of synthetic foam core confined by FRP with impact damage $f_{cc}^{'}$ can be expressed as

$$\frac{f_{cc}^{'}}{f_c} = 1 + k_1 k_s \xi_1 \frac{f_l}{f_c} \tag{19}$$

Substituting Eq. (19) into Eq. (15), the ultimate compressive load capacity of damaged panels without local buckling P_1' is given by

$$P_1' = 0.8\xi_1 f_F A_f + 0.8 f_F A_w + f_c^{'} A_c^{'} + f_c A_c \tag{20}$$

Substituting Eq. (18) into Eq. (16), the ultimate compressive load capacity of damaged panels with local buckling P_2' is given by

$$P_2' = \sigma_{cr}' A_f + 0.8 f_F A_w + f_c^{'} A_c^{'} + f_c A_c \tag{21}$$

The ultimate compressive load capacity of the damaged panels P_u' is the lesser of P_1' and P_2'

$$P_u' = \min\left(P_1^{'}, P_2^{'}\right) \tag{22}$$

Table 3 displayed the comparisons of calculated and experimental results of damaged sandwich panels. The theoretical results are found to be in good agreement with experimental results.

5. Conclusions and the futue work

The impact and post impact behavior of GFRP- synthetic foam sandwich panels were investigated. The results obtained from this study are summarized as follows:

(1) The bare synthetic foam panels exhibited a circular dent on the impacted face for the fiber architecture of the proposed foam panels. The shape of damaged area of sandwich panels under impacting is relative to the applied impact energy and the number of layers in GFRP facesheets. The GFRP- synthetic foam sandwich panels have a diamond shape of damaged area for specimens with 2 or 4 layers of facesheets after 41J-impact due to the fracture of fibers in orthogonal directions. Further increasing the number of GFRP layers or impact energy results in a circular damage on the facesheets. The MPD of sandwich panels is much smaller than that of bare synthetic foam panels, and the sandwich panels with webs have a smaller MPD than

the panels without webs.

(2) The cracks of damaged synthetic foam panels are initiated at the impact dent due to the stress concentration in this region, then propagated in both transversal and vertical directions. The damaged sandwich panels without webs are failed predominantly by debonding between facesheets and core. In contrast, delamination and local buckling of facesheets are occurred in sandwich panels with webs.

(3) When the compressive load of synthetic foam panels is increased up to its peak value,, the panels lost their load carrying capacities suddenly. The sandwich panels without webs exhibit a four-phase displacement: linear-elastic phase, plastic phase, foam compaction phase and facesheets buckling phase. Moreover, the plastic deformation of sandwich panels with webs is much larger than that of panels without webs. After 108J-impact, the reduction of ultimate load of damaged bare synthetic foam panels is less than 8% in comparison with the undamaged panels, while, the ultimate load of damaged sandwich panels with and without webs after 108J-impact is reduced from 8% to 14%.

(4) The proposed analytical model, considered the effects from impact damage, local buckling of FRP facesheets and the confined strength of synthetic foam core, is able to accurately predict the residual ultimate edgewise compressive load capacity of sandwich panels with lattice webs.

In the future, a recently developed computational damage mechanics approach, extended cohesive damage model (ECDM) [34, 35] can be employed to investigate detailed damage evolution in such synthetic foam sandwiches thus directly predict their failure mechanism, loading capacity and residual stiffness in the design stage.

Acknowledgments

The financial support from the National Natural Science Foundation of China (Grant 51578283) and Modern Science and Technology Support Program of Jiangsu Construction Industry of China (Grant 2017-13) is greatly appreciated. Partial funding of this research was provided by the U.S. National Science Foundation Grant IIP 1230351

Reference

[1] Walsh J, Kim H, Suhr J. Low velocity impact resistance and energy absorption of environmentally friendly expanded cork core-carbon fiber sandwich composites. Composites Part A: Applied Science and Manufacturing, 2017, 101:290-296.

[2] Jun Wang, Hota GangaRao, Ruifeng Liang, Weiqing Liu.Experimental and analytical responses of hollow and concrete filled GFRP tube columns under impact. ASCE Journal of Composites for Construction, 2017, 2017, 21(4), 04017013-1 to 15.

[3] Satasivam S, Bai Y. Mechanical performance of bolted modular GFRP composite sandwich structures using standard and blind bolts. Composite Structures, 2014, 117: 59-70

[4] Ude AU, Ariffin AK, Azhari CH. Impact damage characteristics in reinforced woven natural silk/epoxy composite face-sheet and sandwich foam, coremat and honeycomb materials. Int J Impact Eng, 2013, 58:31-38.

[5] Gupta Nikhil, Woldesenbet E, Mensah P. Compression properties of synthetic foams: effect of cenosphere radius ratio and specimen aspect ratio. Composites Part A: Applied Science and Manufacturing, 2004, 35(1): 103-111.
[6] Xia F, Wu X. Work on low-velocity impact properties of foam sandwich composites with various facesheets. Journal of Reinforced Plastics and Composites, 2010, 29(7): 1045-1053.
[7] Ugale VB, Singh KK, Mishra NM, Kumar P. Comparative study of carbon fabric reinforced and glass fabric reinforced thin sandwich panels under impact and static loading. Journal of Composite Materials, 2015, 49(1):99-112.
[8] Schubel PM, Luo J, Daniel IM. Impact and post impact behavior of composite sandwich panels. Composites Part A, 2007, 38: 1051-1057.
[9] Edgren F, Asp LE, Bull PH. Compressive failure of impacted NCF composite sandwich panels-characterisation of the failure process. J Compos Mater, 2004, 38(6): 495-514.
[10] Davies Gao, Hitchings D, Besant T, Clarke A, Morgan C. Compression after impact strength of composite sandwich panels. Compos Struct, 2004:63-1-9.
[11] Zhu S, Chai GB. Damage and failure mode maps of composite sandwich panel subjected to quasi-static indentation and low velocity impact. Composite Structures, 2013, 101: 204-214.
[12] Yang B, Wang Z, Zhou L, Zhang J, Tong L, Liang W. Study on the low-velocity impact response and CAI behavior of foam-filled sandwich panels with hybrid facesheet. Composite Structures, 2015, 132: 1129-1140.
[13] Castanie B, Aminanda Y, Bouvet C, Barrau J. Core crush criterion to determine the strength of sandwich composite structures subjected to compression after impact. Composite Structures, 2008, 86: 243-250.
[14] Nettles A. Normalizing impact energy by face sheet thickness for composite sandwich structure compression after impact testing. Journal of Sandwich Structures and Materials, 2013, 15(3): 340-358.
[15] Feng D, Aymerich F. Damage prediction in composite sandwich panels subjected to low-velocity impact. Composites Part A, 2013, 52: 12-22.
[16] Sabah SHA, Kueh ABH, Al-Fasih MY. Comparative low-velocity impact behavior of bio-inspired and conventional sandwich composite beams. Composites Science and Technology, 2017, 149: 64-74.
[17] Crupi V, Kara E, Epasto G, Guglielmino E, Aykul H. Prediction model for the impact response of glass fibre reinforced aluminium foam sandwiches. International Journal of Impact Engineering, 2015, 77: 97-107.
[18] Chen Y, Hou S, Fu K, Han X, Ye L. Low-velocity impact response of composite sandwich structures: Modelling and experiment. Composite Structures, 2017, 168: 322-334.
[19] Hassan MZ, Umer R, Balawi S, Cantwell WJ. The impact response of environmental friendly sandwich structures. Journal of Composite Materials, 2014, 48(25): 3083-3090.

[20] Corigliano A, Rizzi E, Papa E. Experimental characterization and numerical simulations of a synthetic-foam/glass-fibre composite sandwich. Composites Science and Technology, 2000, 60: 2169-2180.
[21] Lamanna E, Gupta N, Cappa P, Strbik III OM, Cho K. Evaluation of the dynamic properties of an aluminum synthetic foam core sandwich. Journal of Alloys and Compounds, 2017, 695: 2987-2994.
[22] Kumar SJA, Ahmed KS. Compression behavior and energy absorption capacity of stiffened synthetic foam core sandwich composites. Journal of Reinforced Plastics and Composites, 2013, 32(18): 1370-1379.
[23] Omar MY, Xiang C, Gupta N, Strbik III OM, Cho K. synthetic foam core metal matrix sandwich composite: compressive properties and strain rate effects. Materials Science & Engineering A, 2015, 643: 156-168.
[24] Bardella L, Malanca F, Ponzo P, Panteghini A, Porfiri M. A micromechanical model for quasi-brittle compressive failure of glass-microballoons/thermoset-matrix synthetic foams. Journal of the European Ceramic Society, 2014, 34: 2605-2616.
[25] ASTM D 638:2010. Standard test method for tensile properties of plastics.
[26] ASTM D 695:2015. Standard test method for compressive properties of rigid plastics.
[27] ASTM D 1621:2010. Standard test method for compressive properties of rigid cellular plastics.
[28] ASTM D 7137/7137M: 2012. Standard test method for compressive residual strength properties of damaged polymer matrix composite plates.
[29] Timoshenko SP and Gere JM. Theory of elastic stability, 2nd ed., McGraw-Hill, NewYork, 1961.
[30] Teng JG, Chen JF, Smith ST, Lam L. FRP-strengthened RC structures. Chichester: Wiley, 2002.
[31] Wang, L., Liu, W., Fang, Y., Wan, L., Huo, R. (2016). "Axial crush behavior and energy absorption capability of foam-filled GFRP tubes manufactured through vacuum assisted resin infusion". *Thin-Walled Structures*, 98, 263-273.
[32] Perillo, G., Jorgensen, J.K., Cristiano, R., Riccio, A. (2017). "A numerical/experimental study on the impact and CAI behaviour of glass reinforced composite plates". Appl. Compos. Mater., Doi 10.1007/s10443-017-9628-2.
[33] Cheng, X., Al-Mansour, A.M., and Li, Z. (2009). "Residual strength of stitched laminates after low velocity impact". *J. Reinf. Plast. Compos.*, 28(14), 1679-1688.
[34] X Li and J Chen, An extended cohesive damage model for simulating multicrack propagation in fibre composites, Composite Structures, 143, 1–8, 2016.
[35] X Li and J Chen, A highly efficient prediction of delamination migration in laminated composites using the extended cohesive damage model, Composite Structures, 160, 712–721, 2017.

Table 1. Mechanical properties of GFRP

Property	Value
Tensile strength (MPa)	370
Tensile modulus (GPa)	26
Compressive strength (MPa)	167
Compressive modulus (GPa)	12
Poisson ratio	0.23

Table 2 Summary of test matrix

Specimens	m (g)	P_{max} (kN)	T (ms)	MDD (mm)	MPD (mm)	CAI strength (kN)
S0d-I	338	-	-	-	-	106.62
S0d-II	-	5.92	3.504	15.8	7.028	104.40
S0d-III	-	6.68	3.724	16.0	8.837	103.84
S0d-IV	-	7.86	3.920	16.0	11.280	102.63
S0D-I	360	-	-	-	-	119.04
S0D-II	-	6.02	3.384	15.1	5.432	117.87
S0D-III	-	7.64	3.368	15.6	6.315	114.07
S0D-IV	-	8.03	3.796	16.0	9.535	110.28
S2D-I	432	-	-	-	-	119.62
S2D-II	-	8.87	2.676	11.8	1.592	118.56
S2D-III	-	10.41	3.104	12.1	3.087	115.61
S2D-IV	-	11.26	3.288	15.5	3.512	112.04
S4d-I	483	-	-	-	-	117.83
S4d-II	-	10.97	2.568	11.6	0.397	116.36
S4d-III	-	12.47	2.752	11.9	2.035	112.51
S4d-IV	-	13.38	3.152	15.2	2.962	109.88
S4D-I	506	-	-	-	-	123.39
S4D-II	-	11.49	2.552	10.9	0.386	121.41
S4D-III	-	12.78	2.684	11.7	1.405	120.83
S4D-IV	-	13.83	2.976	13.6	1.624	117.15
S6D-I	578	-	-	-	-	147.79
S6D-II	-	12.43	2.54	10.1	0.263	133.46
S6D-III	-	16.38	2.592	10.3	0.968	131.26
S6D-IV	-	17.50	2.468	11.4	1.142	127.45
S4dW2-I	528	-	-	-	-	150.88
S4dW2-II	-	11.57	2.648	9.1	0.374	139.56
S4dW2-III	-	14.16	2.876	9.3	1.273	133.09
S4dW2-IV	-	14.74	3.056	10.1	1.366	130.13
S4DW2-I	552	-	-	-	-	154.89
S4DW2-II	-	12.23	2.548	8.7	0.312	143.44
S4DW2-III	-	14.42	2.776	8.8	0.897	136.25
S4DW2-IV	-	16.01	2.676	9.0	1.218	134.03
S6dW2-I	602	-	-	-	-	167.64
S6dW2-II	-	12.62	2.620	8.3	0.251	160.04
S6dW2-III	-	16.32	2,648	8.6	0.747	154.68
S6dW2-IV	-	16.23	2.936	8.9	1.061	151.37
S6DW2-I	623	-	-	-	-	174.54
S6DW2-II	-	12.71	2.520	7.8	0.227	170.29
S6DW2-III	-	17.26	2.416	8.1	0.268	164.01
S6DW2-IV	-	18.30	2.852	8.2	0.818	159.83

Note: In the first column, the letter d and D mean the densities of synthetic foams are 450 kg/m^3 and 480kg/m^3, respectively, the letter W means the specimens have longitudinal and transversal webs, the first and second numbers mean the number of FRP layers of the facesheets and webs, respectively, and I, II, III and IV mean the applied impact energy is 0, 43 J, 81 J and 108 J, respectively.

Table 3 Comparison between theoretical and experimental results of ultimate load capacities of undamaged sandwich panels

Specimens	P_1' (kN)	P_2' (kN)	P_u' (kN)	P_t (kN)	$\frac{P_u' - P_t}{P_t} \times 100\%$
S2D-I	165.18	126.70	126.70	119.62	5.9
S4d-I	190.86	123.80	123.80	117.83	5.1
S4D-I	205.31	136.30	138.25	123.39	10.5
S6D-I	245.44	163.02	169.59	147.79	10.3
S4dW2-I	221.79	145.59	145.59	150.88	-3.5
S4DW2-I	234.84	158.64	158.64	154.89	2.4
S6dW2-I	261.92	173.26	173.26	167.64	3.4
S6DW2-I	274.93	186.27	186.27	174.54	6.7

Table 4. Comparison between theoretical and experimental results of ultimate load capacities of damaged sandwich panels

Specimens	P_1' (kN)	P_2' (kN)	P_u' (kN)	P_t (kN)	$\frac{P_u' - P_t}{P_t} \times 100\%$
S2D-II	160.16	125.68	125.68	118.56	6.0
S2D-III	157.15	125.54	125.54	115.61	8.6
S2D-IV	155.15	125.41	125.41	112.04	11.9
S4d-II	180.83	115.62	115.62	116.36	-0.7
S4d-III	174.81	114.56	114.56	112.51	1.8
S4d-IV	170.80	113.50	113.50	109.88	3.3
S4D-II	195.28	130.07	130.07	121.41	7.1
S4D-III	189.26	129.01	129.01	120.83	6.8
S4D-IV	185.25	127.95	127.95	117.15	9.2
S6D-II	230.39	141.98	141.98	133.46	6.4
S6D-III	221.36	138.41	138.41	131.26	5.5
S6D-IV	215.34	134.85	134.85	127.45	5.8
S4dW2-II	209.25	136.53	136.53	139.56	-2.1
S4dW2-III	208.62	127.88	134.18	133.09	-3.9
S4dW2-IV	204.61	127.03	131.33	130.13	-2.4
S4DW2-II	222.30	149.58	149.58	143.44	4.3
S4DW2-III	222.03	141.28	147.23	136.25	3.7
S4DW2-IV	218.02	140.44	144.37	134.03	4.8
S6dW2-II	244.36	154.52	154.52	160.04	-3.5
S6dW2-III	240.73	142.12	148.43	154.08	-8.1
S6dW2-IV	234.71	137.53	141.83	151.37	-9.1
S6DW2-II	257.37	167.52	167.52	170.29	-1.6
S6DW2-III	254.09	155.49	161.43	164.01	-5.2
S6DW2-IV	248.07	150.90	154.84	159.83	-6.0

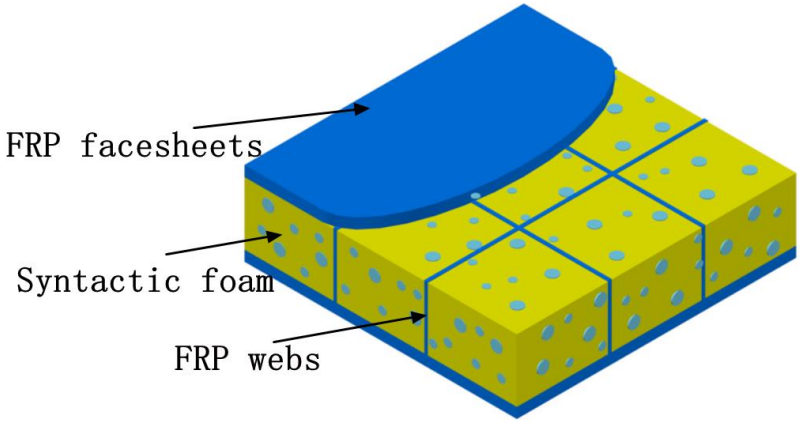

Fig.1 Sketch of FRP-synthetic foam sandwich panels with lattice webs

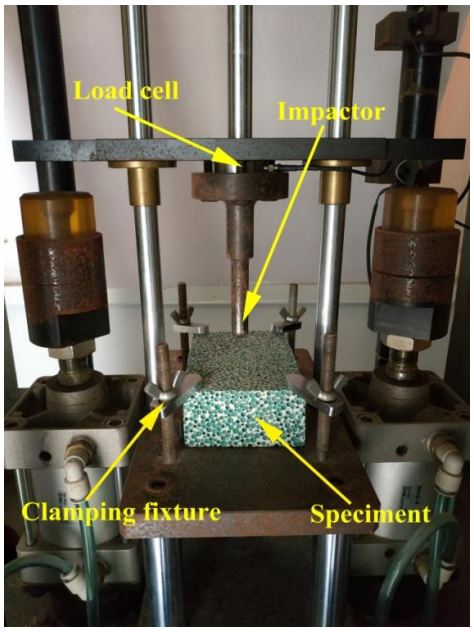

Fig.2 Test set- up of low-velocity impact

Fig.3 Test set-up of edgewise compression

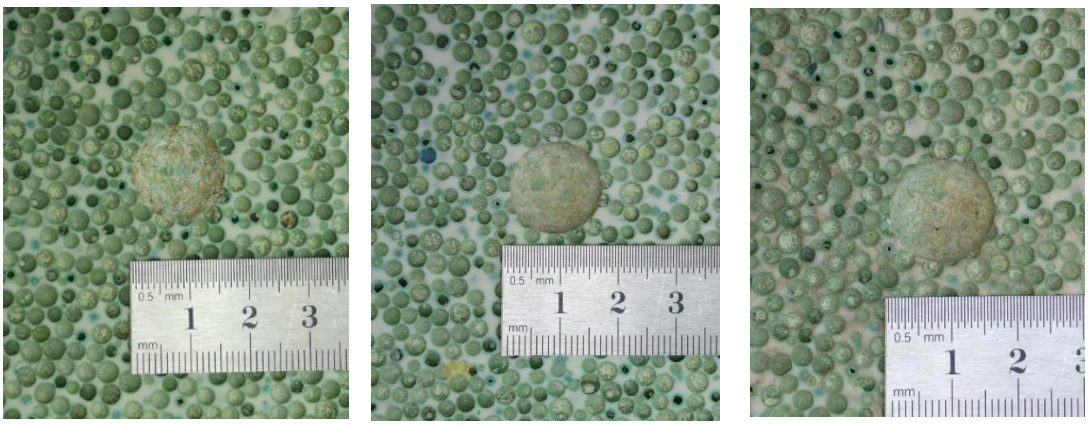

S0d-II S0d-III S0d-IV

(a) Bare synthetic foam panel

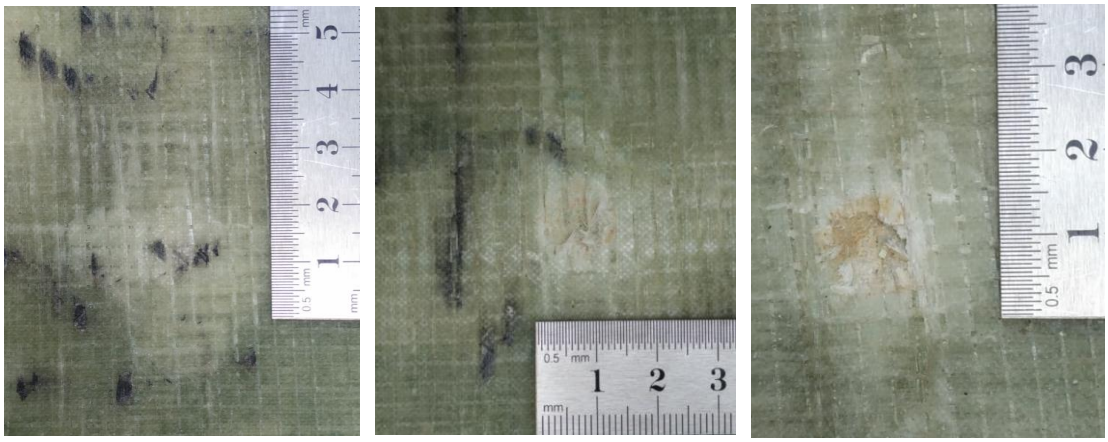

S4d-II S4d-III S4d-IV

(b) GFRP-synthetic sandwich panels

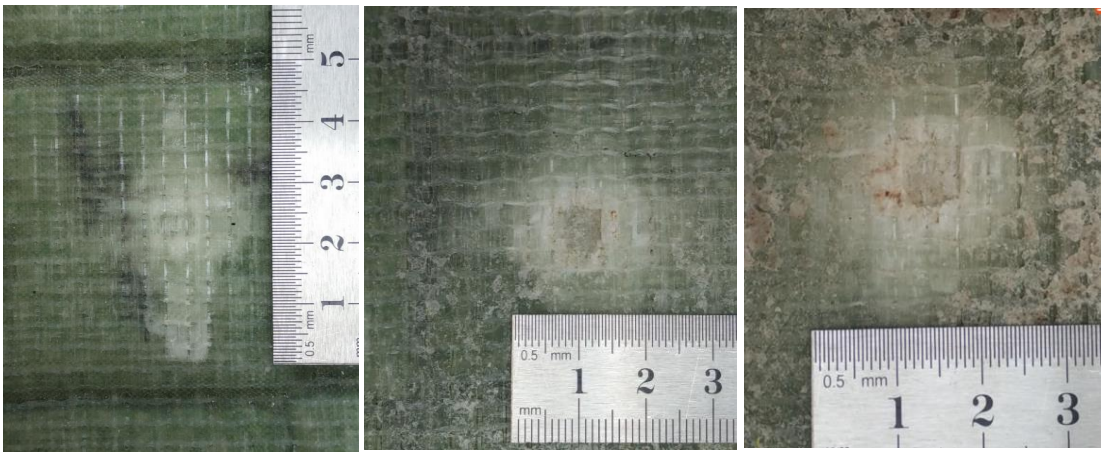

S4dW2-II S4dW2-III S4dW2-IV

(c) GFRP-synthetic sandwich panels with lattice webs

Fig.4 Impact damage of typical specimens

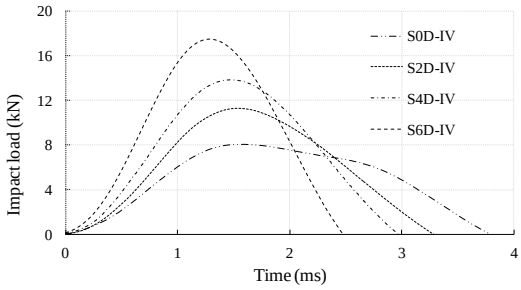

(a) Specimens with different layers in facesheets

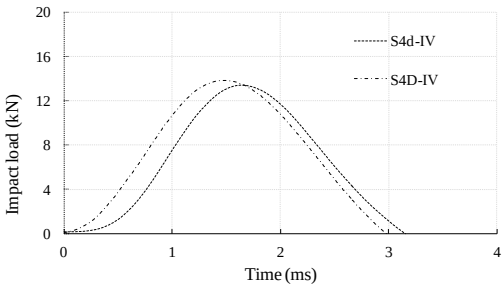

(b) Specimens with different foam density

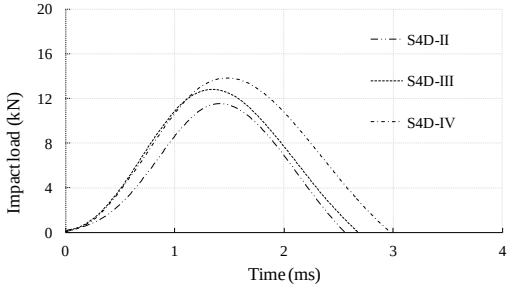

(c) Specimens under different applied energy

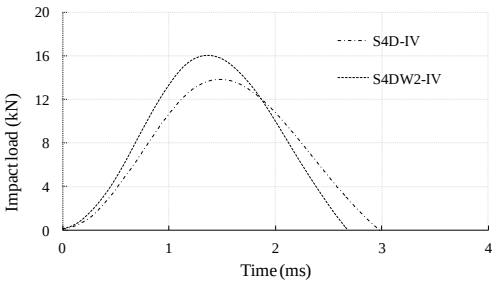

(d) Specimens with and without webs

Fig. 5 Impact load histories

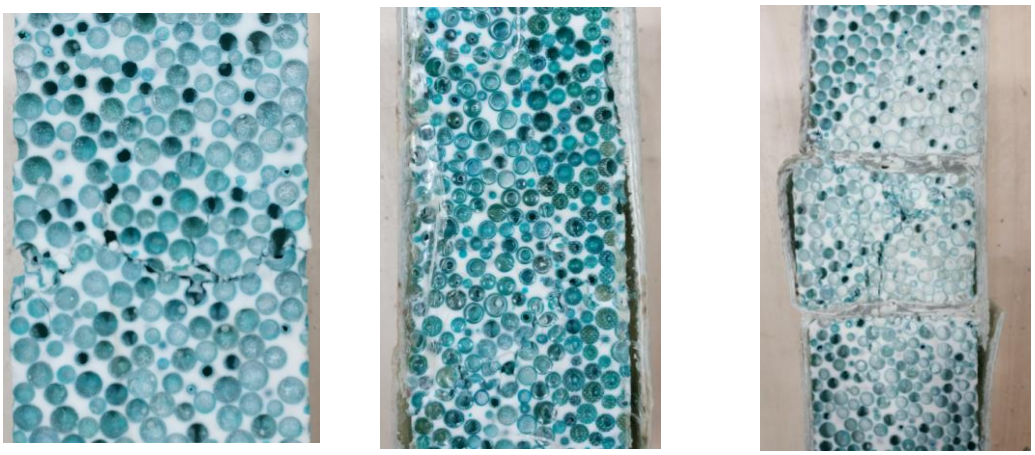

(a) S0D-I (b) S4D-I (c) S4DW2-I

Fig.6 Edgewise compressive failure modes of undamaged specimens

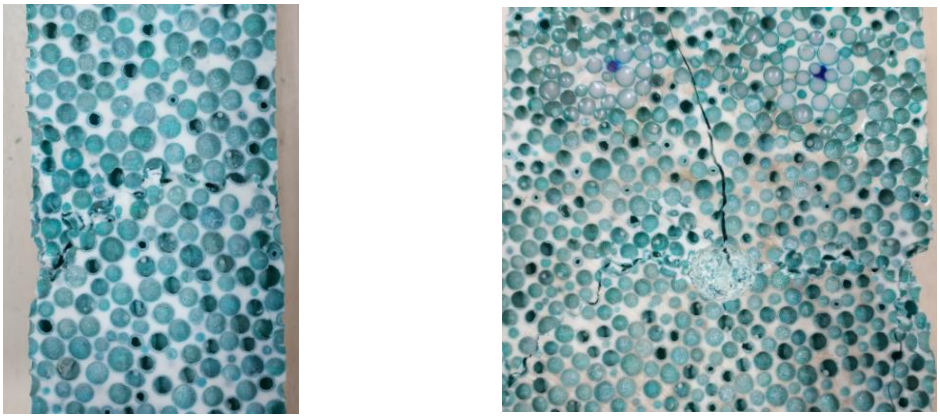

(a) S0D-IV

(b) S4D-IV

(c) S6DW2- IV

Fig.7 Edgewise compressive failure modes of damaged specimens

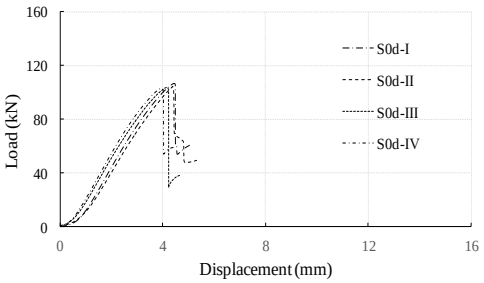

(a) Bare synthetic foam panels

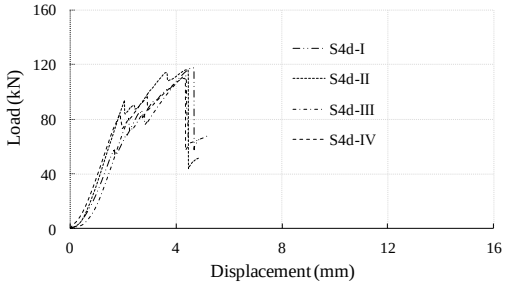

(b) Sandwich panels

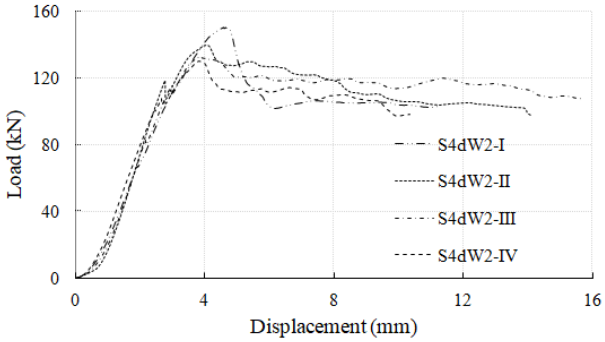

(c) Sandwich panels with webs

Fig.8 Experimental compressive load vs. displacement cures of the investigated specimens

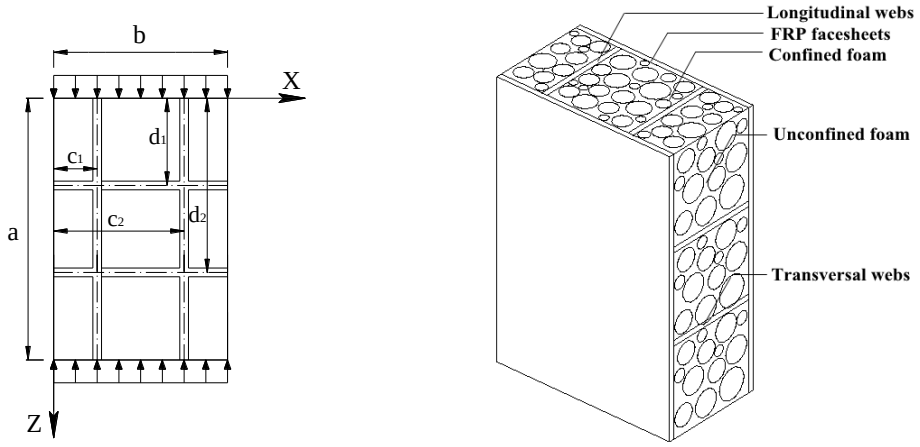

(a) Coordinate system of facesheets

(b) Geometry of sandwich panels with lattice webs

Fig.9 Edgewise Compressive diagram of sandwiches with lattice webs